Theoretical Study on the Group 2 Atoms + N_2O Reactions

Oksana Tishchenko, Christian Vinckier, Arnout Ceulemans, and Minh Tho Nguyen*

Department of Chemistry, University of Leuven, Celestijnenlaan 200F, B-3001 Leuven, Belgium

Received: January 26, 2005; In Final Form: May 9, 2005

The electronic structure aspects of the M (^{1}S,^{3}P) + $N_2O(X^1\Sigma^+)$ (M = Be, Mg, Ca) reactions are investigated using the CASSCF/MRMP2 (complete active space SCF and the multireference Møller−Plesset perturbation theory of the second order) computational methodology. The lowest adiabatic 1 ^{1}A′ and 1 ^{3}A′ potential energy surfaces (PESs) favor the bending dissociation mechanism of N_2O in all studied cases. The rate-limiting channels are determined by the classical barriers that decrease in the series Be (8.9) > Mg (7.0) > Ca (1.2) kcal/mol, whereas the spin-forbidden reaction channels are found to be less important. A comparison with elaborated kinetic results (Plane et al. *J. Phys. Chem.* **1990**, *94*, 5255; *Gas-Phase Metal Reactions*; Elsevier: Amsterdam, 1992; Vinckier et al. *J. Phys. Chem. A* **1999**, *103*, 5328) on the Ca (^{1}S) + $N_2O(X^1\Sigma^+)$ reaction is presented, and the differences in the kinetic behavior of the title reactions are discussed. Our results also indicate that the techniques based on the multiconfigurational wave functions are unavoidable if a correct topology of the PESs governing these reactions is needed.

1. Introduction

In view of its pertinent role in the "global change" context where nitrous oxide is considered as a greenhouse gas and a stratospheric ozone depletion substance,[1] its kinetic behavior has been widely investigated. Particular attention has been paid to its reactions with metal atoms[2] M

$$N_2O(X^1\Sigma^+) + M \rightarrow MO + N_2 \qquad (1)$$

that have recently been proposed as an efficient means of reducing the emission of the greenhouse gas N_2O.[3] Other applications are based on the fact that these reactions are highly exotermic, leading to the product metal oxide formation in the excited states that may cause a strong chemiluminescence. In this way, such reactions can be suitable candidates for the development of chemical lasers in which the population inversion is obtained by means of a pure chemical reaction.[4] The mechanisms and kinetics of these reactions thus form a very interesting topic due to a possibility of the formation of the excited states and in view of the high reaction exothermicities coupled with large values of their Arrhenius activation energies.

To treat the reactions involving metal atoms and to derive reaction cross-sections and activation barriers, two semiempirical models have been proposed. Within the "harpoon" model,[5] the electron jump from a metal atom triggers the ion pair recombination reaction. The reaction cross section then depends on the ionization potentials (IP) of the metal atom and on the electron affinity (EA) of the N_2O molecule. However, as it has been recently shown,[6] the EA^{N_2O} is firmly negative (ca. −6 kcal/mol), which implies that a long-range electron transfer from M to N_2O must be ruled out. The second model is a semiempirical configuration interaction model proposed by Fontijn and coworkers.[7] This model assumes that the reaction of any metal atom with N_2O is governed by the activated complex composed of three resonating structures that are formed by (i) a covalent interaction of the oxygen atom of N_2O with the s-orbital of the metal, (ii) interactions involving excited states of M having a p-character, and (iii) interactions between the ionized species M^+ and N_2O^-. Fairly good correlations were obtained between the theoretical activation barriers and the experimental values.[7d]

Several ab initio and DFT studies on reaction 1 have been performed.[8] Still a major challenge is the treatment of closed shell ns^2 systems such as the group 2 atom/N_2O reactions. There is quite some evidence that these reactions occur along several reaction paths each with its own activation barrier.[9] This may lead in some cases to a non-Arrhenius behavior depending on relative barrier heights and the temperature range covered by the experiment. The purpose of this work is to provide a basic information on the lowest adiabatic singlet and triplet PESs of the title reactions and features of these PESs that control the reaction kinetics.

2. Computational Methods

The multiconfigurational self-consistent field (MCSCF) wave functions of the CASSCF,[10a,b] otherwise referred to as FORS[10c] type, were used throughout this study. The active orbitals, labeled in C_s symmetry, were selected as follows: [8a′−15a′, 1a″−4a″],[12] [12a′−19a′, 2a″−5a″],[12] and [16a′−23a′, 3a″−6a″][12] to describe reaction 1 with M = Be, Mg, and Ca atoms, respectively. The stationary points on the ground (1 ^{1}A′ ≡ ^{1}A′) and the first excited (1 ^{3}A′ ≡ ^{3}A′) PESs were fully optimized and characterized by the harmonic vibrational frequencies at the CASSCF(12/12) level. The lowest energy reaction path was mapped out using the intrinsic reaction coordinate (irc) method to determine the landscape of the studied PESs, and to investigate the triplet state energetics along the lowest energy path on the ^{1}A′ PES. Dynamical electron correlation was accounted for by means of the MRMP2[11] calculations in which all electrons except the 1s were correlated. The O, N, Be, and Mg atomic basis sets were the standard 6-311G basis, supplemented with three d- and one f-type polarization functions, namely, α = 1.02, 0.255, 0.06375, and 0.260, respectively, on

* Corresponding author. E-mail: minh.nguyen@chem.kuleuven.be. Fax: +32 (16) 32 79 92.

10.1021/jp050466+ CCC: $30.25
Published on Web 06/17/2005

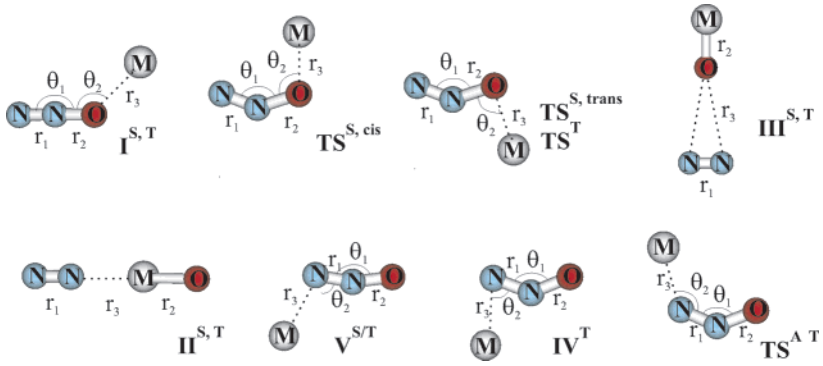

Figure 1. Schematic diagrams of the CASSCF(12/12)-optimized structures relevant to reaction 1.

Be (6-311G(3df)) and $\alpha = 0.70, 0.175, 0.04375, 0.20$, respectively, on Mg (6-311G(3df)), and a single polarization and a diffuse-type function on N and O atoms (6-311+G(d)) to account for a possibility of an electron transfer from metal atoms. All the results presented below for reaction 1 with M = Ca were obtained using the SBKJC effective core potential (ECP) and basis set,[12] referred to hereafter as SBK(d), augmented by single d polarization[13] function on all atoms: $\alpha = 0.8$ on N and O and $\alpha = 0.229$ on Ca. The energy barriers quoted in the text include the harmonic zero-point energy corrections. The results presented below were obtained using the GAMESS[14] and MOLPRO[15] programs.

3. Results and Discussion

The portion of the ^{1}A′ PES that correlates reactants and products of reaction 1 comprises very shallow minima occupied by the weakly bound complexes **I** on the entrance channel, and the linear **II** and the T-shaped **III** complexes (the former resides in the global minimum of the ^{1}A′ PES) on the exit channel. Figure 1 and Table 1 report the molecular geometries of these structures. These reactant and product wells are connected, along the lowest energy channel of reaction 1, via transition state structures $\mathbf{TS}^{S,cis}$ located ca. 8.9 kcal/mol ($\mathbf{TS}^{S,cis}_{Be}$), 7.0 kcal/mol ($\mathbf{TS}^{S,cis}_{Mg}$), and 1.2 kcal/mol ($\mathbf{TS}^{S,cis}_{Ca}$) above the corresponding energy minima **I** on the entrance channel. On the other hand, there exists a higher-energy reaction channel on the ground-state PES through the transition structure $\mathbf{TS}^{S,trans}$ located ca. 15.5, 17.6, and 3.9 kcal/mol above **I** for reaction 1 with Be, Mg, and Ca atoms, respectively. It is worth mentioning that the earlier study on the Mg + N_2O reaction[8d] has found similar reaction pathways on the ^{1}A′ PES with the barriers equal to 11.7 and 23.2 kcal/mol for the lower and higher energy channels, respectively, using the Møller−Plesset second-order perturbation theory (MP2) and the coupled cluster (CCSD(T)) calculations; however, the topology of the studied PES turned out to be rather different: the MP2 (CCSD(T)) methods reveal a two-step mechanism via a stable intermediate cyclic complex NNOMg, but the CASSCF(12/12) PES corresponds to a single-step process. Because at least two electronic configurations are important in the intermediate regions (see, e.g. the molecular orbital (MO) occupation numbers in Figure 2), single-configuration-based methods may result in highly distorted PESs. We therefore consider the results based on the application of the CASSCF(12/12) computational methodology to be likely more accurate.

The portion of the ^{3}A′ PES on the entrance channel of reaction 1 correlating with the $N_2O(X^1\Sigma^+) + M(^3P)$ asymptote comprises energy minima occupied by structures $\mathbf{I}^T$ that, in contrast to the analogous structures $\mathbf{I}^S$ on the ground-state PES, are characterized by shorter M···O distances of 1.818 Å ($\mathbf{I}^T_{Be}$), 2.439 Å ($\mathbf{I}^T_{Mg}$), and 2.370 Å ($\mathbf{I}^T_{Ca}$) (cf. 4.602 Å ($\mathbf{I}^S_{Be}$), 5.330 Å ($\mathbf{I}^S_{Mg}$), and 5.157 Å ($\mathbf{I}^T_{Ca}$)). These energy minima are connected to the reaction products on the ^{3}A′ PES via transition structures $\mathbf{TS}^T$. In fact, small energy barriers $\mathbf{I}^T \rightarrow \mathbf{TS}^T$ on the CASSCF-(12/12) PESs disappear when the dynamic electron correlation is taken into account. This indicates that reaction 1 with M = Be, Mg, Ca along the ^{3}A′ PES is virtually barrierless, because no s−p promotion energy, which is necessary for the intrinsic barrier formation in the group 2 + N_2O reactions, is required on the ^{3}A′ PES. A surprisingly high activation energy of 9.9 kcal/mol for the Mg(^{3}P) + N_2O reaction has been found in a time-resolved laser pumping experiment.[16] Consistent with the earlier ab initio study by Yarkony,[8a] the present calculations show the absence of the barrier in this case, and this is in line

TABLE 1: CASSCF(12/12)-Optimized Structures Relevant to Reaction 1

structure[a]	r_1	r_2	r_3	θ_1	θ_2	energy[b]
$\mathbf{I}^S_{Be}$	1.116	1.203	4.602	180.0	87.0	0.0
$\mathbf{I}^S_{Mg}$	1.131	1.204	5.330	180.0	103.1	0.0
$\mathbf{I}^S_{Ca}$	1.143	1.231	5.157	180.0	148.6	0.0
$\mathbf{I}^T_{Be}$	1.104	1.235	1.818	177.0	116.5	49.3
$\mathbf{I}^T_{Mg}$	1.111	1.217	2.439	178.9	126.3	55.2
$\mathbf{I}^T_{Ca}$	1.134	1.246	3.370	177.9	135.6	36.0
$\mathbf{TS}^{S,cis}_{Be}$	1.122	1.278	1.783	149.8	106.9	9.5
$\mathbf{TS}^{S,cis}_{Mg}$	1.137	1.278	2.219	143.7	98.0	7.9
$\mathbf{TS}^{S,cis}_{Ca}$	1.151	1.287	2.349	152.1	112.9	2.2
$\mathbf{TS}^{S,trans}_{Be}$	1.107	1.300	1.653	158.7	165.3	16.0
$\mathbf{TS}^{S,trans}_{Mg}$	1.122	1.319	2.102	148.8	91.2	19.0
$\mathbf{TS}^{S,trans}_{Ca}$	1.143	1.299	2.190	155.4	111.1	5.0
$\mathbf{TS}^{T}_{Be}$	1.109	1.258	1.722	165.1	103.5	45.9
$\mathbf{TS}^{T}_{Mg}$	1.118	1.265	2.148	157.2	103.7	53.5
$\mathbf{TS}^{T}_{Ca}$	1.139	1.273	2.254	161.2	118.3	34.5
$\mathbf{II}^S_{Be}$	1.104	1.340	1.735			−97.6
$\mathbf{II}^S_{Mg}$	1.106	1.756	2.481			−22.3
$\mathbf{III}^T_{Be}$	1.073	1.476	3.771			−51.2
$\mathbf{III}^T_{Mg}$	1.107	1.897	3.614			−18.2
$\mathbf{V}^{S/T}_{Mg}$	1.210	1.270	2.204	133.2	122.5	24.0
$\mathbf{V}^{S/T}_{Ca}$ [c]	1.294	1.268	2.200	123.8	79.0	6.8
$\mathbf{IV}^T_{Be}$	1.214	1.229	1.522	133.8	141.1	−3.3
$\mathbf{IV}^T_{Mg}$	1.234	1.258	2.059	136.4	80.1	22.7
$\mathbf{IV}^T_{Ca}$	1.255	1.298	2.273	134.5	76.2	−1.0
$\mathbf{TS}^{a,T}_{Be}$	1.198	1.296	1.625	129.8	95.9	13.8
$\mathbf{TS}^{a,T}_{Mg}$	1.210	1.270	2.040	133.2	122.4	28.6
$\mathbf{TS}^{a,T}_{Ca}$	1.230	1.317	2.196	130.4	133.1	3.9

[a] The bond lengths (r) are given in ångstroms; the bond angles (θ), in degrees. For the definition of the geometrical parameters see Figure 1. [b] The MR-MP2 energies with respect to the structure **I** ($E(^{MRMP2}\mathbf{I}^S_{Be})$ = −198.888617 au, $E(^{MRMP2}\mathbf{I}^S_{Mg})$ = −384.047841 au, $E(^{MRMP2}_{ECP}\mathbf{I}^S_{Ca})$ = −36.098282 au), in kcal/mol, without correction for zero-point energy. [c] $\mathbf{V}^{S/T}_{Ca}$ structure optimized at the CASSCF(6/6) level.

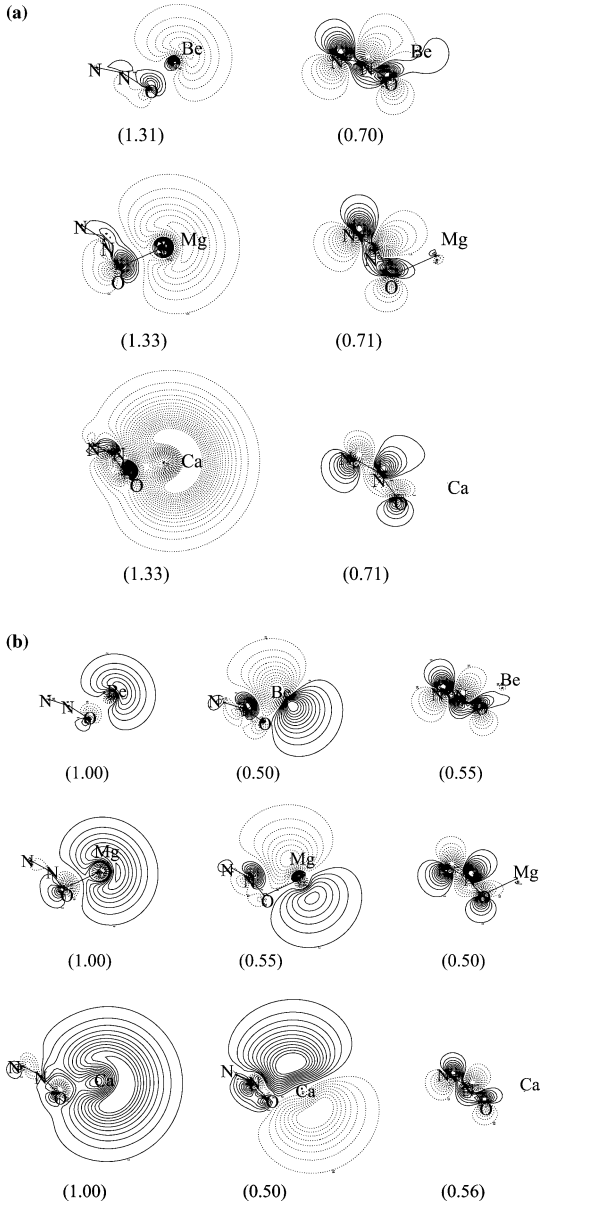

Figure 2. Shape of the "key" MOs (SA-CASSCF natural set) at the transition state geometries of the $M(^1S) + N_2O(X^1\Sigma^+)$ (a) and $M(^3P) + N_2O(X^1\Sigma^+)$ (b) reactions. Numbers in parentheses indicate electron occupancies.

with the large reaction cross section measured by Dagdigian[17] (see also discussion in ref 9b). Geometrically, the triplet $\mathbf{TS}^T$ are rather similar to their singlet $\mathbf{TS}^{S,trans}$ counterparts but appear to be more reactant-like. In particular, the M···O and N···O distances and the NNO angle are equal to 1.722 Å, 1.258 Å, and 165° in $\mathbf{TS}^T_{Be}$ (cf. 1.653 Å, 1.300 Å, and 158.8° in $\mathbf{TS}^S_{Be}$), 2.148 Å, 1.265 Å, and 157° in $\mathbf{TS}^T_{Mg}$ (cf. 2.102 Å, 1.319 Å, and 148° in $\mathbf{TS}^S_{Mg}$), and 2.254 Å, 1.273 Å, and 161° in $\mathbf{TS}^T_{Ca}$ (cf. 2.190 Å, 1.299 Å, and 155° in $\mathbf{TS}^S_{Ca}$) (see Table 1).

The electron rearrangement process in the transition state regions involves a charge transfer from either the s- or p-orbital of the ^1S ($\mathbf{TS}^S$) or ^3P ($\mathbf{TS}^T$) metal atom, respectively, to the in-plane $2p-\pi$ orbital of N_2O. This is reflected in the changes of the electronic configuration of the ground adiabatic state from the neutral to a charge-transfer ionic one when passing over these barriers. The key molecular orbitals (MOs) that significantly change their occupation numbers are shown in Figure 2. The structure of the wave functions in the intermediate regions indicates that the ground adiabatic state is dominated by both the "neutral" and the "ionic" configurations. These configurations are of utmost importance in the Fontijn model, which is apparently successful[7d] in prediction of the potential barriers heights.

Because the $N_2O(X^1\Sigma^+) + Mg(^1S)$ reaction yields the MgO product in both singlet and triplet states,[9a] it is essential to know where the crossing between the $^1A'$ and $^3A'$ PES takes place. If the crossing occurs at the entrance channel, it could dramatically affect the reaction rate and its temperature dependence. To address this question, the $^3A'$ energetics has been mapped as a function of the irc on the $^1A'$ PES. The results indicate that along the lowest energy reaction pathway, the crossing does not occur at the entrance channel, where the singlet−triplet energy separation is rather large (the singlet−triplet energy gap at the $\mathbf{TS}^S$ geometry is equal to ca. 6 kcal/mol). However, it may take place at the exit channel associated with the ionic portion of the ground-state PES, i.e., after the passage over the $\mathbf{TS}^S$ structure, as schematically shown in Figure 3a. This indicates that the reaction along its lowest energy channel is likely to be described using conventional terms.

Because it has previously been assumed that the lowest reaction barrier arises from the crossing of a singlet and a triplet PESs,[9a] the present study has in particular been focused on the investigation of this possibility, i.e., on the search of the $^1A'/^3A'$ crossing at the entrance channel. The results indicate that

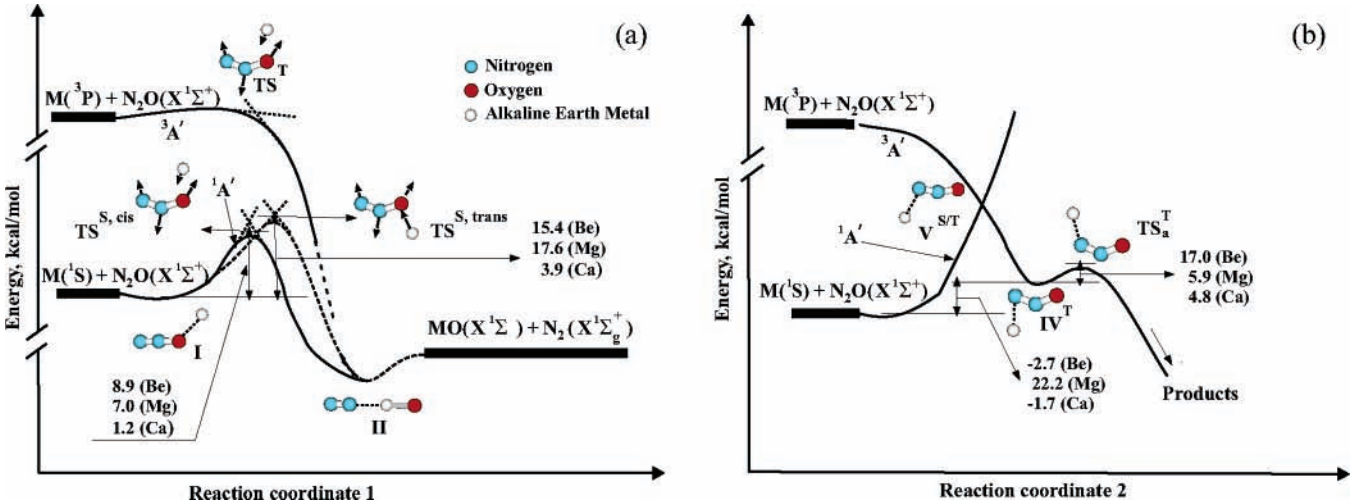

Figure 3. Schematic representation of the potential energy profile of reaction 1 along its spin-allowed (a) and spin-forbidden (b) reaction channels. The zero of energy corresponds to the ground-state reactant asymptote.

the $^3A'$ PES actually crosses the entrance channel of reaction 1 at higher energies as compared to the minimum energy path, as indicated in Figure 3b. The energy-minimized crossing point $\mathbf{V}_{Mg}^{S/T}$ on the $^1A'/^3A'$ crossing seam, which can be regarded as a local minimum on the seam, has been located at $r_1 = 1.210$ Å, $r_2 = 1.270$ Å, $r_3 = 2.204$ Å, $\theta_1 = 133°$, and $\theta_1 = 123°$. It is characterized by a rather stretched N−N bond of 1.210 Å, as compared to the transition state structure (cf. Table 1) and also a rather bent N−N−O moiety. Energetically, the $\mathbf{V}_{Mg}^{S/T}$ structure is placed ca. 24 kcal/mol above $\mathbf{I}_{Mg}^{S}$, implying that it is not accessible under the experimental conditions employed in refs 9b and 19. By way of contrast, the analogous $\mathbf{V}_{Ca}^{S/T}$ structure ($r_1 = 1.230$ Å, $r_2 = 1.334$ Å, $r_3 = 2.263$ Å, $\theta_1 = 117°$, $\theta_1 = 72°$) is placed 4.5 kcal/mol above the lowest lying saddle point, $\mathbf{TS}_{Ca}^{S,cis}$, and could be part of the reaction mechanism. Note that the $\mathbf{V}^{S/T}$ structures were obtained at the CASSCF level with subsequent energy evaluations using MRMP2, where the states remain (nearly) degenerate. A re-optimization of the corresponding structures at the correlated levels of theory might lower their energies with respect to the asymptotes. The rest of the nonadiabatic pathway via the singlet−triplet crossing takes place on the ionic portion of the $^3A'$ PES, which exhibits a potential minimum at structure **IV**. The later is connected to the reaction products by the transition structure $\mathbf{TS}_a^T$ with energy barriers of 17.0 kcal/mol (M = Be), 5.9 kcal/mol (M = Mg), and 4.8 kcal/mol (M = Ca).

Summarizing, we conclude that there are actually at least four distinct reaction pathways of reaction 1, namely

$$M(^1S) + N_2O(X^1\Sigma^+) \rightarrow \mathbf{I^S} \rightarrow \mathbf{TS^{S,cis}} \rightarrow \mathbf{II} \rightarrow MO + N_2(X^1\Sigma^+_g) \quad (2)$$

$$M(^1S) + N_2O(X^1\Sigma^+) \rightarrow \mathbf{I^S} \rightarrow \mathbf{TS^{S,trans}} \rightarrow \mathbf{II} \rightarrow MO + N_2(X^1\Sigma^+_g) \quad (3)$$

$$M(^3P) + N_2O(X^1\Sigma^+) \rightarrow \mathbf{I^T} \rightarrow \mathbf{TS^T} \rightarrow \mathbf{II} \rightarrow MO + N_2(X^1\Sigma^+_g) \quad (4)$$

$$M(^1S) + N_2O(X^1\Sigma^+) \rightarrow \mathbf{V^{S/T}} \rightarrow \mathbf{IV^T} \rightarrow \mathbf{TS_a^T} \rightarrow MO + N_2(X^1\Sigma^+_g) \quad (5)$$

Obviously, reaction pathway 2 is the most favorable. The resulting barrier height of 1.2 kcal/mol for the Ca reaction is in fairly good agreement with the value of 1.6 kcal/mol derived from the kinetic data.[9e] The experimental data on the Mg (^1S) + N_2O activation energy turn out to be rather uncertain. Although the earlier study of Brekenridge et al.[18] estimated its magnitude in the range 15−20 kcal/mol, subsequent measurements in our group[19] and the measurements by Plane et al.[9b] resulted in lower values of 10.6 and 9.6 kcal/mol, respectively (cf. also 9.2 kcal/mol determined as the threshold translational energy).[9a] Overall, the reaction barrier to the Mg reaction is consistently much higher as compared to the lowest energy barrier of the Ca reaction. We are not aware of any previous reports on the Be + N_2O reaction. The calculated barrier heights of M(^1S) + N_2O reactions decrease in the same order as decrease the ionization potentials of M atoms: $IP^{Be} = 9.32 > IP^{Mg} = 7.65 > IP^{Ca} = 6.11$ eV.[2]

Although the reaction with Mg atoms shows a simple Arrhenius behavior, the analogous reaction with Ca atoms exhibits a pronounced non-Arrhenius regime. The presence of a curvature on the Arrhenius plot is usually associated with a mechanistic changeover due to an activation of higher-energy reaction channels that gain their importance as temperature increases. Though there exist distinct reaction channels with appreciably different activation barriers in both the Mg + N_2O and Ca + N_2O reactions, the reaction channels with higher activation energies are only accessible in the latter case. The nonlinear least-squares fits of the two-channel model rate equation to the data for the Ca reaction resulted in the reaction barriers for the two different reaction channels of 1.2 and 5.4 kcal/mol[9e] that are in favorable agreement with the reaction barrier heights of 1.2 and 3.9 kcal/mol in reaction channels 2 and 3 obtained in the present work. From these theoretical barriers Arrhenius activation energies for both channels can be calculated to be 1.7 and 4.4 kcal/mol, respectively. With these Arrhenius parameters a statistical analysis was performed on the experimental data[9e] of the rate constant k_{Ca/N_2O} as a function of the temperature. As one can see in Figure 4, a fairly good agreement was obtained for the temperatures below 750 K with a determination coefficient $R^2 = 0.955$. The overall expression is given in following equation:

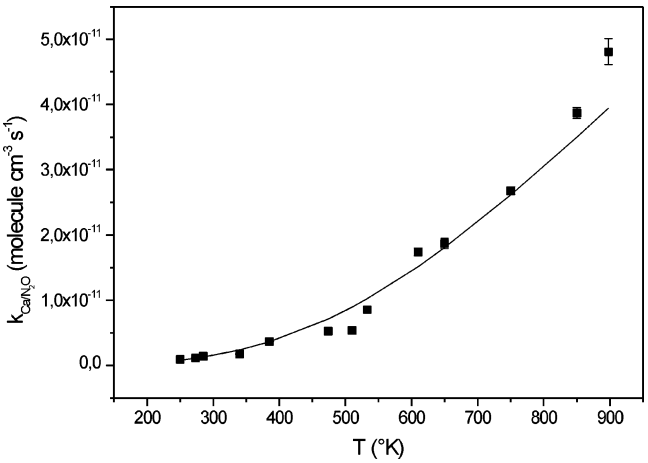

Figure 4. Comparison between experimentaly determined rate constant k_{Ca/N_2O}[9e] and fitted values on the basis of the two channel path (eq 6).

$$k_{Ca/N_2O} = (3.6 \pm 0.07) \times 10^{-10} \exp(-4.4 \text{ kcal mol}^{-1}/RT) + (2.1 \pm 0.03) \times 10^{-11} \exp(-1.7 \text{ kcal mol}^{-1}/RT) \quad (6)$$

It should be pointed out, however, that at the increased temperatures the value of k_{Ca/N_2O} is underestimated by eq 6, especially if also the measurements up to 1015 K of ref 9d are taken into account. This deviation is due presumably to the contributions of the reaction mechanisms that involve nonadiabatic transitions betwen the ground and the first excited singlet and/or triplet PESs and implies that the latter cannot be neglected in the modeling of the reaction in the broad temperature range. Note that the preexponential factor in the first term of this expression differs by about a factor of 10 from the preexponential factor in the second term. Taking proper account of the alternative reaction mechanisms that contribute at higher energies may significantly alter this result.

A striking non-Arrhenius behavior displayed by similar reactions has been attributed in the past to an increase of a vertical electron affinity of the N_2O molecule under the excitation of its doubly degenerate bending mode, which enables a close-range electron transfer to occur at the elevated temperatures.[20] Our preliminary CASSCF(12/12) calculations indicate the presence of a seam of conical intersection of the ground 1 $^1A'$ and the first excited 2 $^1A'$ PESs in the N_2O + M systems at nuclear arrangements characterized by a strongly bent NNO

moiety. The energy-minimized point on this 1 $^1A'/2\ ^1A'$ seam in the N_2O + Ca system is found at $r_{NN} = 1.226$ Å, $r_{NO} = 1.557$ Å, $r_{CaO} = 2.290$ Å, $\theta_{NNO} = 119.5°$, and $\theta_{CaNO} = 71.8°$, $dih_{CaNNO} = 180°$. The presence of a conical intersection between these two PESs that describe the "neutral" and "ionic" reactants offers a support to this earlier interpretation and adds further insight into the role of the electron-transfer mechanism in the process. However, a more elaborate study is required to explore this possibility in a quantitative way.

From the above, the following major conclusions should be emphasized: (i) the reactivities of M(^{1}S) and M(^{3}P) atoms toward N_2O are strikingly different; (i) the lowest $^1A'$ and $^3A'$ PESs that correlate reactants to products favor the bending dissociation mechanism of N_2O in all studied cases; (iii) although the topology of the low lying PESs of the group 2 + N_2O reactions appear to be rather similar, the magnitude of the barrier heights on the $^1A'$ are remarkably different. In the Mg + N_2O case, only the lowest adiabatic reaction channel via the saddle point $\mathbf{TS}^{S,cis}$ with the barrier of 7.0 kcal/mol is accessible under the experimental conditions employed in studies.[9b,19] By way of contrast, at least three different reaction channels could be operative in the temperature range 300−1000 K employed in the previous studies on the Ca + N_2O reaction. These are the two adiabatic channels via $\mathbf{TS}^{S,cis}$ and $\mathbf{TS}^{S,trans}$ with activation barriers of 1.2 and 3.9 kcal/mol, respectively, and the reaction path through a singlet−triplet intersection located a few kcal/mol above the reactant energy minimum. We believe that these results will augment the mechanistic picture of reaction 1 derived from the experimental data.

Acknowledgment. The continuing support of the Belgian Government (GOA program) and the KU Leuven Research Council is gratefully acknowledged. We thank one of the reviewers for many helpful comments.

References and Notes

(1) Prather, M.; Ehhalt, D. H. *Chemistry of the Greenhouse Gases* In *Climate Change 2001: the Scientific Base*; Houghto, J. T., et al., Eds.; Cambridge University Press: New York, 2001.

(2) *NIST Standard Reference Database 69—March 2003 Release: NIST Chemistry WebBook.*

(3) Perry, R. A.; Miller, J. A. *Int. J. Chem. Kinet.* **1996**, *28*, 217.

(4) (a) Cool, T. A. *Rection Dynamics*. (b) Smith, I. W. M., Ed. *Physical Chemistry of Fast Reactions 2*; Plenum Press: New York, 1980; p 215. (c) Herbelin, J. M.; Cohen, N. *J. Quant. Spectrosc. Radiat. Transfer* **1975**, *15*, 731.

(5) (a) Polanyi, M. *Atomic Reactions*; Williams and Norgate: London, 1932. (b) Herschbach, D. R. *Adv. Chem. Phys.* **1966**, *10*, 319.

(6) Kryachko, E. S.; Vinckier, C.; Nguyen, M. T. *J. Chem. Phys.* **2001**, *114*, 7911.

(7) (a) Fontijn, A. *Pure Appl. Chem.* **1998**, *70*, 469. (b) Futerko, P. M.; Fontijn, A. *J. Phys. Chem.* **1991**, *95*, 8065. (c) Futerko, P. M.; Fontijn, A. *J. Phys. Chem.* **1993**, *98*, 7004. (d) Fontijn, A.; Futerko, P. M. In *Gas-Phase Metal Reactions*; Fontijn, A., Ed.; Elsevier: Amsterdam, 1992 (see also references therein).

(8) (a) Yarkony, D. R. *J. Chem. Phys.* **1983**, *78*, 6763. (b) Stirling, A. *J. Am. Chem. Soc.* **2001**, *124*, 4058. (c) Delabie, A.; Vinckier, C.; Flock. M.; Pierloot, K. *J. Phys. Chem.* **2001**, *105*, 5479. (d) Kiran, B.; Vinckier, C.; Nguyen, M. T. *Chem. Phys. Lett.* **2001**, *344*, 213. (e) Kryachko, E. S.; Tishchenko, O.; Nguyen, M. T. *Int. J. Quantum Chem.* **2002**, *89*, 329. (f) Tishchenko, O.; Kryachko, E. S.; Vinckier, C.; Nguyen, M. T. *Chem. Phys. Lett.* **2002**, *363*, 550. (g) Tishchenko, O.; Vinckier, C.; Nguyen, M. T. *J. Phys. Chem. A* **2004**, *108*, 1268.

(9) (a) Naulin, C.; Costes, M.; Moudden, Z.; Dorthe, G. *J. Phys. Chem* **1991**, *95*, 8244. (b) Plane J. M. C.; Nien, C. F.; Rajasekhar, B. *J. Phys. Chem.* **1992**, *96*, 1296. (c) Plane, J. M. C. In *Gas-Phase Metal Reactions*; Fontijn, A., Ed.; Elsevier: Amsterdam, 1992. (d) Vinckier, C.; Helaers, J.; Remeysen, J. *J. Phys. Chem. A* **1999**, *103*, 5328. (e) Plane, J. M. C.; Nien, C. F. *J. Phys. Chem.* **1990**, *94*, 5255.

(10) (a) Roos, B. O.; Taylor, P. *Chem. Phys.* **1980**, *48*, 157−173. (b) Werner, H.-J.; Knowles, P. J. *J. Chem. Phys.* **1985**, *82*, 5053. (c) Ruedenberg, K.; Schmidt, M. W.; Gilbert, M. M.; Elbert, S. T. *Chem. Phys.* **1982**, *71*, 41.

(11) (a) Hirao, K. *Chem. Phys. Lett.* **1992**, *190*, 374−380. (b) Hirao, K. *Chem. Phys. Lett.* **1992**, *196*, 397. (c) Hirao, K. *Chem. Phys. Lett.* **1993**, *201*, 59−66. (d) Hirao, K. *Int. J. Quantum Chem.* **1992**, Suppl. *26*, 517−526.

(12) (a) Stevens, W. J.; Basch, H.; Krauss, M. *J. Chem. Phys.* **1984**, *81*, 6026. (b) Stevens, W. J.; Krauss, M.; Basch, H.; Jasien, P. J. *Can. J. Chem.* **1992**, *70*, 612. (c) Cundari, T. R.; Stevens, W. J. *J. Chem. Phys.* **1993**, *98*, 5555.

(13) Hariharan, P. C.; Pople, J. A. *Theor. Chim. Acta* **1973**, *28*, 213.

(14) Schmidt, M. W.; Baldridge, K. K.; Boatz, J. A.; Elbert, S. T.; Gordon, M. S.; Jensen, J. H.; Koseki, S.; Matsunaga, N.; Nguyen, K. A.; Su, S. J.; Windus, T. L.; Dupuis, M.; Montgomery, J. A. *J. Comput. Chem.* **1993**, *14*, 1347−1363.

(15) Werner, H.-J.; Knowles, P. J. version 2002.1, Amos, R. D.; Bernhardsson, A.; Berning, A.; Celani, A.; Cooper, D. L.; Deegan, M. J. O.; Dobbyn, A. J.; Eckert, F.; Hampel, C.; Knowles, P. J.; Korona, T.; Lindh, R.; Lloyd, A. W.; McNicholas, S. J.; Mandy, F. R.; Meyer, W.; Mura, M. E.; Nicklass, A.; Palmieri, P.; Pitzer, R.; Rauhut, G.; Schütz, M.; Schumann, U.; Stoll, H.; Stone, A. J.; Tarroni, R.; Thorsteinsson, T.; Werner, H.-J. MOLPRO, a package of ab initio programs.

(16) (a) Husain, D.; Schifino, J. *J. Chem. Soc., Faraday Trans. 2* **1982**, *78*, 2083. (b) Husain, D.; Roberts, G. *J. Chem. Soc., Faraday Trans. 2* **1986**, *82*, 395.

(17) Dagdigian, J. P. *J. Chem. Phys.* **1982**, *76*, 5375.

(18) Breckenridge, W. H.; Umemoto, H. *J. Phys. Chem.* **1983**, *87*, 1804.

(19) Vinckier, C.; Christiaens, P. *J. Phys. Chem.* **1992**, *96*, 2146.

(20) Plane, J. M. C. *J. Phys. Chem.* **1987**, *91*, 6552 and references therein.